

## Study of the $^{22}\text{Mg}$ Waiting Point Relevant for X-Ray Burst Nucleosynthesis via the $^{22}\text{Mg}(\alpha, p)^{25}\text{Al}$ Reaction

H. Jayatissa<sup>1,\*</sup>, M. L. Avila,<sup>1</sup> K. E. Rehm,<sup>1</sup> P. Mohr<sup>2</sup>, Z. Meisel,<sup>3</sup> J. Chen,<sup>1</sup> C. R. Hoffman<sup>1</sup>, J. Liang<sup>4,†</sup>,  
C. Müller-Gatermann<sup>1</sup>, D. Neto<sup>5</sup>, W. J. Ong<sup>6</sup>, A. Psaltis<sup>7</sup>, D. Santiago-Gonzalez<sup>1</sup>, T. L. Tang<sup>1,‡</sup>,  
C. Ugalde<sup>5</sup> and G. Wilson<sup>8</sup>

<sup>1</sup>Physics Division, Argonne National Laboratory, Lemont, Illinois 60439, USA

<sup>2</sup>Institute for Nuclear Research (Atomki), P.O. Box 51, Debrecen H-4001, Hungary

<sup>3</sup>Institute of Nuclear and Particle Physics, Ohio University, Athens, Ohio 45701, USA


<sup>4</sup>Department of Physics and Astronomy, McMaster University, Hamilton, Ontario L8S 4M1, Canada

<sup>5</sup>Department of Physics, University of Illinois Chicago, 845 W. Taylor St., Chicago, Illinois 60607, USA

<sup>6</sup>Lawrence Livermore National Laboratory, 7000 East Ave, Livermore, California 94550, USA

<sup>7</sup>Institut für Kernphysik, Technische Universität Darmstadt, Darmstadt D-64289, Germany

<sup>8</sup>Department of Physics and Astronomy, Louisiana State University, Baton Rouge, Louisiana 70803, USA

 (Received 30 October 2022; revised 21 February 2023; accepted 8 August 2023; published 15 September 2023)

The  $^{22}\text{Mg}(\alpha, p)^{25}\text{Al}$  reaction rate has been identified as a major source of uncertainty for understanding the nucleosynthesis flow in Type-I x-ray bursts. We report a direct measurement of the energy- and angle-integrated cross sections of this reaction in a 3.3–6.9 MeV center-of-mass energy range using the MULTi-Sampling Ionization Chamber (MUSIC). The new  $^{22}\text{Mg}(\alpha, p)^{25}\text{Al}$  reaction rate is a factor of  $\sim 4$  higher than the previous direct measurement of this reaction within temperatures relevant for x-ray bursts, resulting in the  $^{22}\text{Mg}$  waiting point of x-ray burst nucleosynthesis flow to be significantly bypassed via the  $(\alpha, p)$  reaction.

DOI: [10.1103/PhysRevLett.131.112701](https://doi.org/10.1103/PhysRevLett.131.112701)

An x-ray burst (XRB) is a thermonuclear explosion in a binary system of an accreting neutron star and a companion star [1–3]. Properties of the neutron star can be deduced from comparisons between the observations of XRB light curves and astrophysical models [4–7]. These models significantly depend on nuclear physics inputs, such as nuclear reaction rates [8,9]. The accretion of hydrogen from the companion star prior to an XRB ensures that the main nucleosynthesis occurs via proton capture on elements formed via the hot carbon-nitrogen-oxygen cycle and its breakout reactions [10]. It has been suggested that the main  $(p, \gamma)$  nucleosynthesis path in XRBs is halted at several “waiting points” [11] due to a  $(p, \gamma)$ - $(\gamma, p)$  equilibrium. Alpha capture reactions could allow the halted nucleosynthesis process to bypass these waiting points to synthesize heavier elements.

One of the waiting points identified for XRB nucleosynthesis is  $^{22}\text{Mg}$  ( $T_{1/2} = 3.876$  s [12]). The interplay between the  $(\alpha, p)$  reaction with the proton capture reaction on  $^{22}\text{Mg}$  and the subsequent  $\beta$  decay plays an important role for the subsequent nucleosynthesis flow. Since the  $Q$  value of the  $^{22}\text{Mg}(p, \gamma)^{23}\text{Al}$  reaction is small ( $Q$  value = 0.141 MeV) [13], a  $(p, \gamma)$ - $(\gamma, p)$  equilibrium is established [6], and capture reactions will occur within timescales that are short compared to the half life of  $^{22}\text{Mg}$ . Hence, the reaction flow through the  $^{22}\text{Mg}$  waiting point is mainly determined by the  $^{22}\text{Mg}(\alpha, p)^{25}\text{Al}$  reaction and the proton capture rate on  $^{23}\text{Al}$

created via  $^{22}\text{Mg}(p, \gamma)^{23}\text{Al}$  reaction. The uncertainties on the proton capture rate on  $^{23}\text{Al}$  have recently been substantially reduced experimentally [14,15]. Currently, the  $^{22}\text{Mg}(\alpha, p)^{25}\text{Al}$  reaction rate provides the main uncertainty in constraining the nucleosynthesis flow at the  $^{22}\text{Mg}$  waiting point, despite recent experimental efforts. Moreover, sensitivity studies have identified the  $^{22}\text{Mg}(\alpha, p)^{25}\text{Al}$  reaction to significantly impact the XRB light curves and burst ashes [8,16].

Several experiments have been carried out to constrain the  $^{22}\text{Mg}(\alpha, p)^{25}\text{Al}$  reaction rate [17–19]. An indirect measurement was carried out by Matic *et al.* [17] using the  $^{28}\text{Si}(p, t)^{26}\text{Si}$  reaction to study the level structure of  $^{26}\text{Si}$ . This work identified four resonances in  $^{26}\text{Si}$  above the  $\alpha$ -decay threshold ( $Q_\alpha = 9.166$  MeV), with unknown spins and parities. Because of the limited information obtained in this work, the  $^{22}\text{Mg}(\alpha, p)^{25}\text{Al}$  rate was deduced with large uncertainties and it was found to be several orders of magnitude lower than the predictions using the Hauser-Feshbach (HF) [20] formalism. Therefore, the experimental reaction rate was considered to be a lower limit by the authors. Later, the first direct measurement of the  $^{22}\text{Mg}(\alpha, p)^{25}\text{Al}$  reaction was performed in inverse kinematics by Randhawa *et al.* [18]. This work utilizes recoil protons measured within a limited angular range and the fusion-evaporation code PACE4 [21] to extract the angle-integrated cross sections in a center-of-mass energy

range of 3.2–10.6 MeV. An uncertainty of  $\sim 35\%$  was estimated in the cross sections due to the uncertainty from the model prediction of the proton angular distributions. To fit the low reaction cross sections and to extrapolate them down to the center-of-mass energies relevant for XRBs, the HF code TALYS [22] was used with notable modifications to the radius of the  $\alpha$ -particle optical model potential, and a significant increase of the default  $^{26}\text{Si}$  level density. When compared to the HF predictions using NON-SMOKER [23], the total reaction cross sections were a factor of  $\approx 8$  lower. Recently, Hu *et al.* [19] carried out a measurement of the  $^{25}\text{Al} + p$  (in)elastic scattering reaction and studied states relevant to the  $^{22}\text{Mg}(\alpha, p)^{25}\text{Al}$  reaction in the excitation energy range of 9.166–11 MeV (above the  $\alpha$ -decay threshold). This work performed an R-matrix fit to assign spins and parities of the states observed. The partial  $\alpha$  widths of four resonances above the  $\alpha$ -decay threshold in  $^{26}\text{Si}$  were inferred from the mirror nucleus  $^{26}\text{Mg}$ . After taking into account the energy shift of  $\sim 300$  keV determined by Refs. [24] and [25], the energy range studied by Hu *et al.* corresponds to an energy range of  $\sim 9.5$ –11.3 MeV in  $^{26}\text{Mg}$ . Surprisingly, the number of measured resonances is low when compared with the almost 90 known levels in the same excitation energy range of the mirror nucleus  $^{26}\text{Mg}$  [26]. Assuming that at least half of these levels in  $^{26}\text{Mg}$  have unnatural parity, the number of expected candidate levels in  $^{26}\text{Si}$  is a factor of  $\sim 10$  higher than those measured by Hu *et al.* [19]. Thus, the rate from this work should be considered as a lower limit. The  $^{22}\text{Mg}(\alpha, p)^{25}\text{Al}$  reaction rate from that experiment is a factor of 8 to 10 lower than that obtained from NON-SMOKER for  $\sim 0.4$ –1 GK, and increases up to a factor of  $\sim 160$  at 3 GK. For temperatures below 1 GK, this rate is in agreement with that by Randhawa *et al.* [18]. From the low reaction rate found by these two previous measurements, Ref. [19] concluded that the XRB reaction flow follows mainly the  $^{22}\text{Mg}(p, \gamma)^{23}\text{Al}(p, \gamma)^{24}\text{Si}$  path, implying that the  $^{22}\text{Mg}$  waiting point is potentially not bypassed. Further astrophysical implications of the low  $^{22}\text{Mg}(\alpha, p)^{25}\text{Al}$  rate from this work can be found in Ref. [27].

In this Letter, we present a new independent study of the  $^{22}\text{Mg}(\alpha, p)^{25}\text{Al}$  reaction that directly measures angle- and energy-integrated cross sections, removing the model dependence for obtaining the total cross sections, common to all previous measurements. A direct measurement of the  $^{22}\text{Mg}(\alpha, p)^{25}\text{Al}$  reaction in inverse kinematics was performed using the Argonne Tandem Linac Accelerator System (ATLAS) at Argonne National Laboratory. A radioactive beam of  $^{22}\text{Mg}^{12+}$  was developed with the ATLAS in-flight system [28] using the  $^{20}\text{Ne}(^3\text{He}, n)^{22}\text{Mg}$  reaction with a primary beam of  $^{20}\text{Ne}$  at an energy of 125.0 MeV. The  $^{22}\text{Mg}$  beam, with an energy of  $74.0 \pm 1.5$  MeV, and an average intensity of 200 pps was delivered to the MULTi-Sampling Ionization Chamber (MUSIC) detector [29] filled with 404 Torr of pure He gas. The  $^{22}\text{Mg}$  beam energy was determined using a silicon detector upstream of MUSIC and

confirmed by the known magnetic rigidity of an upstream beam-line transport dipole magnet. The silicon detector calibration was based on the measured energy of the unreacted  $^{20}\text{Ne}$  beam as determined by the ATLAS time-of-flight system. The main contaminants of the  $^{22}\text{Mg}$  beam include different charge states of the primary  $^{20}\text{Ne}$  beam and a small amount of  $^{22}\text{Na}^{10+}$ . The ratio of  $^{22}\text{Mg}$  to contaminants was about 18%. Using the energy deposited in the Frisch grid and the first anode strip, the  $^{22}\text{Mg}$  beam can be counted and separated from these contaminants.

Energy loss tables are used to calculate the energy of the beam at each of the anode strips of the detector. In order to identify the best energy loss table for the present work, a silicon detector was placed downstream of MUSIC to measure the remaining  $^{22}\text{Mg}$  beam energy. Since the beam stops inside the detector for the He gas pressure used for this measurement, the pressures were lowered to allow the  $^{22}\text{Mg}$  beam to go through the gas and exit window foil. The gas pressures used ranged from 0 to 250 Torr in steps of 50 Torr. The beam energies measured with this silicon detector were well reproduced using energy loss calculations performed using the ATIMA 1.2 [30] energy loss tables. This was also cross-checked via its reproducibility of the Bragg peak in the energy loss of the beam inside MUSIC for the 404 Torr gas pressure used for the final measurement. This work presents a direct  $^{22}\text{Mg}(\alpha, p)^{25}\text{Al}$  cross section measurement in the center-of-mass energy range of 3.3–6.9 MeV.

The MUSIC detector is sensitive to the energy loss of a particle as it travels through the gas and has the ability to measure an excitation function with a single beam energy. When a reaction occurs at any anode strip, differences in the energy deposited can be used to separate out the  $(\alpha, p)$  events of interest from the other reaction channels. Summing the energy deposited in various numbers of consecutive strips using a  $\Delta E - \Delta E$  technique after a reaction occurs allows for further separation of the different reaction channels (see Ref. [31]). More information on using MUSIC for direct  $\alpha$ -induced measurements can be found in Refs. [31–35]. For the energy range covered in this work, the  $(\alpha, \gamma)$ ,  $(\alpha, p)$ ,  $(\alpha, 2p)$ , elastic  $(\alpha, \alpha)$ , and inelastic  $(\alpha, \alpha')$  channels are energetically allowed. The MUSIC detector cannot distinguish the  $(\alpha, 2p)$  reaction due to indistinguishable energy losses from other  $(\alpha, \alpha)$  or  $(\alpha, \alpha')$  channels.

For the center-of-mass energies corresponding to each strip, the total  $(\alpha, p)$  cross section can be obtained by normalizing the total number of  $(\alpha, p)$  events identified for each strip to the measured beam intensity. The corresponding statistical and systematic uncertainties of the cross sections from the present work are tabulated in Table I. Here, the effective center-of-mass energies ( $E_{\text{c.m.}}^{\text{eff}}$ ) have been adjusted to take into account the energy dependence of the cross sections over the target thickness for each data point. The uncertainties of  $E_{\text{c.m.}}^{\text{eff}}$  is defined by the

TABLE I. Total reaction cross sections,  $\sigma$ , and associated systematic and statistical uncertainties obtained from the present measurement for the  $^{22}\text{Mg}(\alpha, p)^{25}\text{Al}$  reaction for center-of-mass energies corresponding to anode strips 2-12 of MUSIC.

$E_{\text{c.m.}}^{\text{eff}}$ (MeV)	$\Delta E_{\text{c.m.}}^{\text{a}}$ (MeV)	$\sigma$ (mb)	$\Delta\sigma_{\text{sys}}$ (mb)	$\Delta\sigma_{\text{stat}}$ (mb)
6.93 (28)	+0.17 -0.17	91	11	11
6.60 (29)	+0.18 -0.18	127	15	14
6.25 (29)	+0.18 -0.18	111	7	13
5.91 (30)	+0.19 -0.19	102	6	12
5.55 (31)	+0.19 -0.20	75	5	10
5.19 (31)	+0.19 -0.21	111	7	13
4.82 (32)	+0.20 -0.23	71	4	10
4.44 (33)	+0.20 -0.24	57	3	9
4.06 (33)	+0.19 -0.26	36	4	7
3.67 (34)	+0.18 -0.29	26	3	6
3.25 (35)	+0.18 -0.30	14	2	4

<sup>a</sup>The energy binning per strip is determined by the energy loss of the  $^{22}\text{Mg}$  beam along the width of each corresponding strip.

uncertainty of the beam energy. The estimated energy loss of the beam within each anode strip defines the energy binning  $\Delta E_{\text{c.m.}}$ . The systematic uncertainty of the cross sections arises predominantly from the analysis techniques and conditions used to separate the  $(\alpha, p)$  events from the beam and other reaction channels. This separation becomes more difficult at the beginning of the detector and as the reaction vertex gets closer to the Bragg peak of the beam. Thus higher systematic uncertainties ( $\sim 12\%$ ) are assigned for the first two and last three energy points.

Figure 1 shows the total reaction cross sections of only  $^{22}\text{Mg}(\alpha, p)^{25}\text{Al}$  obtained from the present work in comparison with the direct measurement of Ref. [18] and scaled theoretical HF calculations. The NON-SMOKER cross sections have been divided by a factor of 8 to reproduce the data of Ref. [18]. However, it is important to note that the NON-SMOKER calculations do not differentiate between the contributions from the  $(\alpha, p)$  and  $(\alpha, 2p)$  channels, which do not represent these experimental data. The total reaction cross section using TALYS were calculated using the  $\alpha$ -particle optical model potential by McFadden and Satchler [36], which has been shown to work well for masses  $20 \lesssim A \lesssim 50$  [37]. The statistical model [20] distributes the total cross section  $\sigma$  among the open reaction channels in the energy range under study. The contribution of the  $(\alpha, \gamma)$  channel to the cross section remains very minor ( $\approx 5$  orders of magnitude smaller). The theoretical  $^{25}\text{Al}$  production cross section in the  $^{22}\text{Mg}(\alpha, p)^{25}\text{Al}$  reaction, as measured by MUSIC, was calculated by the sum over the final states in  $^{25}\text{Al}$ ;  $\sigma(^{25}\text{Al}) = \sum_i b_i \sigma(\alpha, p_i)$  where the branchings  $b_i$  describe the probability that the  $i$ th excited state in  $^{25}\text{Al}$  finally

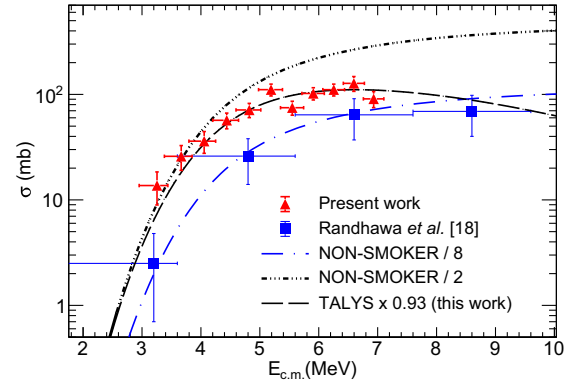


FIG. 1. Experimental cross sections for  $^{22}\text{Mg}(\alpha, p)^{25}\text{Al}$  from the present measurement (red triangles) and the data from Ref. [18] (blue squares). Also shown are the theoretical HF cross section calculations using TALYS  $\times 0.93$  for  $(\alpha, p)$  only (dash black line), along with NON-SMOKER/8 (dot-dash blue line) and NON-SMOKER/2 (dot-dot-dot-dash black line), which includes both  $(\alpha, p)$  and  $(\alpha, 2p)$ .

decays to the ground state;  $(1 - b_i)$  corresponds to the probability that the  $i$ th state decays by proton emission. In practice,  $b_i = 1$  for all states below the proton binding energy in  $^{25}\text{Al}$  of 2.27 MeV, and  $b_i \approx 0$  for most states above 2.27 MeV; only a few states above 2.27 MeV with high  $J^\pi$  decay preferentially by  $\gamma$  emission to the ground state of  $^{25}\text{Al}$ . It has been seen from the present study that such manual summing of the different exit channels in combination with the dominating  $(\alpha, p)$  and  $(\alpha, 2p)$  channels makes the calculation almost insensitive to other ingredients of the statistical model like the gamma-ray strength function, the level density, or the proton optical model potential. This theoretical cross section reproduces the energy dependence of the new experimental data quite well. For the best reproduction of the new data, the theoretical  $^{25}\text{Al}$  production cross sections have been scaled down by a factor of 0.93, which is well within the expected uncertainty of a factor of 2. As seen in Fig. 1, for the lowest center-of-mass energies ( $\lesssim 2.5$  MeV), these TALYS cross sections are similar to those from NON-SMOKER divided by a factor of 2, but differ at higher energies due to a larger contribution of the  $(\alpha, 2p)$  channel that is not subtracted in NON-SMOKER. See Supplemental Material [38] for a more in-depth explanation of the applicability of TALYS for the  $^{22}\text{Mg}(\alpha, p)^{25}\text{Al}$  reaction.

Some observed deviations between theory and experiment could be explained by the presence of strong resonances or due to a higher level density. For instance, the two cross section data points at 5.19 and 5.55 MeV covering center-of-mass energies of 4.98–5.74 MeV show deviations from the TALYS predictions. A rough correspondence to resonances in  $^{22}\text{Ne}(\alpha, n)^{25}\text{Mg}$  mirror reaction [39,40] can be found, taking into account the energy shift of  $\sim 300$  keV between mirror states in  $^{26}\text{Mg}$  and  $^{26}\text{Si}$ .



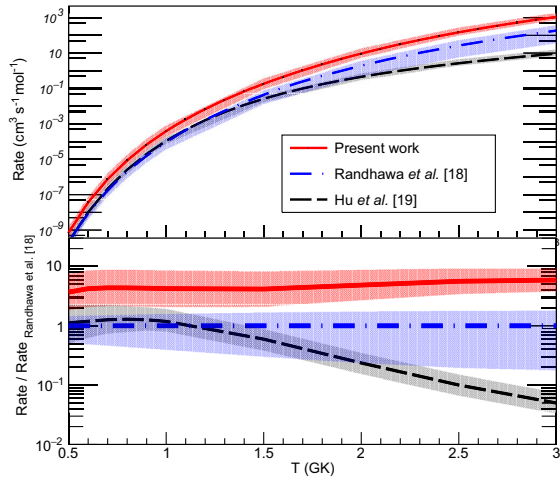


FIG. 2. Upper panel: The  $^{22}\text{Mg}(\alpha, p)^{25}\text{Al}$  reaction rate based on this work in comparison to the rates from Randhawa *et al.* [18] and Hu *et al.* [19]. Lower panel: The same reaction rates as a ratio to the rate by Randhawa *et al.* [18].

The present work provides an experimental reaction rate corresponding to the upper end of the Gamow window for  $T \approx 1.8$  GK. To extrapolate the rate to lower temperatures, the experimental total reaction cross sections were combined with the TALYS predictions at lower energies with an uncertainty of a factor of 2 (see Ref. [38] for details). The resulting geometric mean reaction rate was calculated using the code Exp2Rate [41], and is shown in Fig. 2 (red solid line) along with the rates from Randhawa *et al.* [18] (blue dot dashed line) and Hu *et al.* [19] (black dashed line). A table with the recommended reaction rates, the upper and lower limits, and the fitted parameters to the REACLIB format can be found in the Supplemental Material [38]. As can be seen in Fig. 2, the  $^{22}\text{Mg}(\alpha, p)^{25}\text{Al}$  reaction rate from the present work is significantly higher than those by Refs. [18] and [19]. The factor of  $\approx 4$  between the new  $^{22}\text{Mg}(\alpha, p)^{25}\text{Al}$  rate and that of Randhawa *et al.* reflects the factor of  $\approx 4$  between the reaction cross sections for  $E_{\text{c.m.}} \leq 3$  MeV. Although not understood, this discrepancy could be associated to the model dependency of the obtained angle-integrated cross section in Ref. [18]. The discrepancy with the measurement of Ref. [19] can be explained by the low number of states measured in their work. As discussed before, when compared to the mirror reaction, the number of candidate levels that could potentially contribute is expected to be about a factor of  $\sim 10$  higher. A possible reason could be that resonances in  $^{26}\text{Si}$  may decay by proton emission to excited states in  $^{25}\text{Al}$ , resulting in a weak signal in the excitation curve of proton elastic scattering. Hence, resonances with small  $\Gamma_{p0}$  in  $^{26}\text{Si}$  may remain below the detection limit of [19]. Additionally, the energy interval measured by Ref. [19] in  $^{26}\text{Si}$  only covers up to  $\sim 1$  GK, explaining the larger discrepancy at higher temperatures.

The implications of the new  $^{22}\text{Mg}(\alpha, p)^{25}\text{Al}$  reaction rate for XRB model calculations and the flow through the  $^{22}\text{Mg}$

waiting point are discussed below. The impact on the flow into the  $\alpha p$  process can be calculated by using the two reactions affecting the destruction of  $^{22}\text{Mg}$ : namely  $^{22}\text{Mg}(\alpha, p)^{25}\text{Al}$  and  $^{23}\text{Al}(p, \gamma)^{24}\text{Si}$  as previously described. The flow can then be defined as  $\lambda_{(\alpha, p)} / (\lambda_{(\alpha, p)} + \lambda_{(p, \gamma)})$ , where  $\lambda_i = W_i \rho N_A \langle \sigma v \rangle X_{\text{fuel}} / A_{\text{fuel}}$  with  $A_{\text{fuel}}$  and  $X_{\text{fuel}}$  being the mass number and the mass fraction of hydrogen and helium for the  $^{23}\text{Al}(p, \gamma)^{24}\text{Si}$  and  $^{22}\text{Mg}(\alpha, p)^{25}\text{Al}$  reactions, respectively [42]. Here,  $W_i$  is a weight factor that determines the equilibrium abundance of a nuclide calculated using the Saha equation for a given temperature. In order to obtain the relevant temperatures and mass fractions, the model by Merz and Meisel [42] was adopted, where the observed features of the x-ray clockburst *GS 1826-24* [43] were reproduced for an ignition occurring at  $T = 0.7$  GK with  $X_{\text{H}} = 0.06$  and  $X_{\text{He}} = 0.19$  and a peak temperature ( $T_{\text{peak}}$ ) at 1.0 GK. The nucleosynthesis flow into the  $\alpha p$  process for temperatures ranging from the ignition point to peak temperatures are of interest.

For the following discussion, this work considers a 10% flow as the onset point or the point when the  $\alpha p$  process becomes significant (as was done in Ref. [14]) and considers a flow greater than 50% as a significant bypass of the  $^{22}\text{Mg}$  waiting point via the  $(\alpha, p)$  reaction. The  $^{23}\text{Al}(p, \gamma)^{24}\text{Si}$  reaction rate used for the flow calculations are from a recent high-precision mass measurement of  $^{24}\text{Si}$  that significantly reduced the previous rate uncertainties [14]. The calculated nucleosynthesis flow into the  $\alpha p$  process presented in Fig. 3 shows that the previous  $^{22}\text{Mg}(\alpha, p)^{25}\text{Al}$  rates by Randhawa *et al.* and Hu *et al.* results in a relatively minor flow into the  $\alpha p$  process at  $^{22}\text{Mg}$  (ranging from 3% to 51% even at  $T_{\text{peak}} = 1$  GK) for the relevant temperatures, indicating that the  $^{22}\text{Mg}$  waiting point is potentially not bypassed. Using the results from the present work, the flow into the  $\alpha p$  process is significant

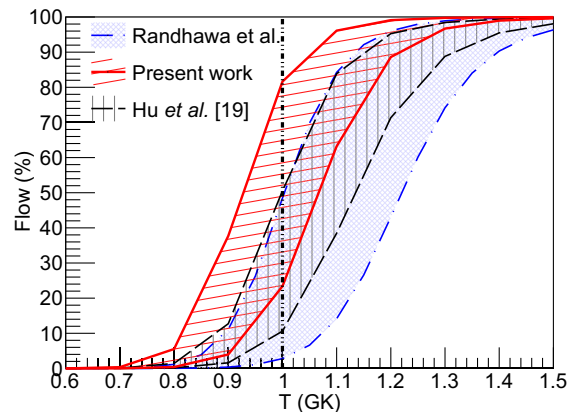


FIG. 3. The upper and lower bounds of the flow into the  $\alpha p$  process calculated using the ignition conditions of Merz and Meisel [42] ( $X_{\text{H}} = 0.06$ ,  $X_{\text{He}} = 0.19$ ) using the  $^{22}\text{Mg}(\alpha, p)^{25}\text{Al}$  rates from the present work (red solid lines), Hu *et al.* (black dashed line), and Randhawa *et al.* (blue dot-dashed line). The vertical line denotes the peak temperature for the model by Ref. [42].

with at least 23% and as high as 82% at 1 GK. In addition, this new rate suggests that the onset of the  $\alpha p$  process occurs at a lower temperature  $T_9 = 0.87 \pm 0.06$ , while the onset temperatures using the rates of Randhawa *et al.* and Hu *et al.* occurs at  $T_9 = 0.99 \pm 0.09$  and  $T_9 = 0.94 \pm 0.06$ , respectively, which is close to the peak temperature. The enhanced flow through the  $^{22}\text{Mg}(\alpha, p)^{25}\text{Al}$  path directly impacts the shape of the light curve by decreasing the luminosity early in the burst due to reduced hydrogen burning. This reduction in hydrogen burning during the initial stages leads to a larger amount of hydrogen available for burning at later times, resulting in a less pronounced decline in the light curve tail. However, since the amplitudes of the new  $^{22}\text{Mg}(\alpha, p)^{25}\text{Al}$  reaction rate fall between the rates calculated using NON-SMOKER and those of Refs. [18] and [19], significant changes to the light curve presented in Ref. [18] are not expected.

This work presents a new direct measurement of the angle- and energy-integrated cross sections of the  $^{22}\text{Mg}(\alpha, p)^{25}\text{Al}$  reaction, which was found to be a factor of  $\approx 4$  higher than the previous direct measurement. The new reaction rate shows a significant nucleosynthesis flow into the  $\alpha p$  process at the  $^{22}\text{Mg}$  waiting point, contradicting recent results that found this to be relatively minor with the main nucleosynthesis flow occurring via  $^{22}\text{Mg}(p, \gamma)^{23}\text{Al}(p, \gamma)^{24}\text{Si}$ . In addition, this work found that the onset of the  $^{22}\text{Mg}(\alpha, p)^{25}\text{Al}$  reaction occurs at lower temperatures.

The Supplemental Material [38] provides the following additional references: [44–63]. This material is based upon work supported by the U.S. Department of Energy, Office of Science, Office of Nuclear Physics, under Contract No. DE-AC02-06CH11357, and National Research Development and Innovation Office (NKFIH), Budapest, Hungary (K134197). This research used resources of Argonne National Laboratory’s ATLAS facility, which is a DOE Office of Science User Facility. A. P. also acknowledges support from the Deutsche Forschungsgemeinschaft (DFG, German Research Foundation)-Project No. 279384907-SFB 1245, and the State of Hesse within the Research Cluster ELEMENTS (Project ID 500/10.006). This was work performed under the auspices of the U.S. Department of Energy by Lawrence Livermore National Laboratory under Contract No. DE-AC52-07NA27344. This work was supported by the U.S. Department of Energy Office of Science under Grant No. DE-FG02-88ER40387 and DE-SC0019042 and the U.S. National Nuclear Security Administration through Grant No. DE-NA0003909.

\*Corresponding author: [hjayatissa@anl.gov](mailto:hjayatissa@anl.gov)

<sup>†</sup>Present address: TRIUMF, Vancouver, British Columbia, V6T 2A3, Canada.

<sup>‡</sup>Present address: Department of Physics, Florida State University, Tallahassee, Florida 32306, USA.

- [1] W. H. G. Lewin, J. van Paradijs, and R. E. Taam, *Space Sci. Rev.* **62**, 223 (1993).
- [2] H. Schatz and K. E. Rehm, *Nucl. Phys.* **A777**, 601 (2006).
- [3] A. Parikh, J. José, G. Sala, and C. Iliadis, *Prog. Part. Nucl. Phys.* **69**, 225 (2013).
- [4] H. Schatz, A. Aprahamian, J. Görres, M. Wiescher, T. Rauscher, J. Rembges, F.-K. Thielemann, B. Pfeiffer, P. Möller, K.-L. Kratz, H. Herndl, B. Brown, and H. Rebel, *Phys. Rep.* **294**, 167 (1998).
- [5] J. L. Fisker, H. Schatz, and F.-K. Thielemann, *Astrophys. J. Suppl. Ser.* **174**, 261 (2008).
- [6] Z. Meisel, A. Deibel, L. Keek, P. Shternin, and J. Elfritz, *J. Phys. G* **45**, 093001 (2018).
- [7] Z. Meisel, *Astrophys. J.* **860**, 147 (2018).
- [8] R. H. Cyburt, A. M. Amthor, A. Heger, E. Johnson, L. Keek, Z. Meisel, H. Schatz, and K. Smith, *Astrophys. J.* **830**, 55 (2016).
- [9] Z. Meisel, G. Merz, and S. Medvid, *Astrophys. J.* **872**, 84 (2019).
- [10] M. Wiescher, J. Görres, and H. Schatz, *J. Phys. G* **25**, R133 (1999).
- [11] J. L. Fisker, F.-K. Thielemann, and M. Wiescher, *Astrophys. J. Lett.* **608**, L61 (2004).
- [12] M. S. Basunia, *Nucl. Data Sheets* **127**, 69 (2015).
- [13] W. J. Huang, M. Wang, F. G. Kondev, G. Audi, and S. Naimi, *Chin. Phys. C* **45**, 030002 (2021).
- [14] D. Puentes, Z. Meisel, G. Bollen, A. Hamaker, C. Langer, E. Leistenschneider, C. Nicoloff, W.-J. Ong, M. Redshaw, R. Ringle, C. S. Sumithrarachchi, J. Surbrook, A. A. Valverde, and I. T. Yandow, *Phys. Rev. C* **106**, L012801 (2022).
- [15] G. Lotay *et al.*, *Phys. Lett. B* **833**, 137361 (2022).
- [16] R. H. Cyburt, A. M. Amthor, R. Ferguson, Z. Meisel, K. Smith, S. Warren, A. Heger, R. D. Hoffman, T. Rauscher, A. Sakharuk, H. Schatz, F. K. Thielemann, and M. Wiescher, *Astrophys. J. Suppl. Ser.* **189**, 240 (2010).
- [17] A. Matic *et al.*, *Phys. Rev. C* **84**, 025801 (2011).
- [18] J. S. Randhawa *et al.*, *Phys. Rev. Lett.* **125**, 202701 (2020).
- [19] J. Hu *et al.*, *Phys. Rev. Lett.* **127**, 172701 (2021).
- [20] W. Hauser and H. Feshbach, *Phys. Rev.* **87**, 366 (1952).
- [21] O. B. Tarasov and D. Bazin, *Nucl. Instrum. Methods Phys. Res., Sect. B* **376**, 185 (2016).
- [22] A. Koning and D. Rochman, *Nucl. Data Sheets* **113**, 2841 (2012).
- [23] T. Rauscher (NON-SMOKER Collaboration), <http://nuastro.org/nonsmoker.html>.
- [24] A. Matic *et al.*, *Phys. Rev. C* **82**, 025807 (2010).
- [25] D. Seweryniak, P. J. Woods, M. P. Carpenter, T. Davinson, R. V. F. Janssens, D. G. Jenkins, T. Lauritsen, C. J. Lister, J. Shergur, S. Sinha, and A. Woehr, *Phys. Rev. C* **75**, 062801(R) (2007).
- [26] ENSDF database, <https://www.nndc.bnl.gov/ensdf/>.
- [27] Y. H. Lam, Z. X. Liu, A. Heger, N. Lu, A. M. Jacobs, and Z. Johnston, *Astrophys. J.* **929**, 72 (2022).
- [28] C. Hoffman, T. Tang, M. Avila, Y. Ayyad, K. Brown, J. Chen, K. Chipps, H. Jayatissa, B. Kay, C. Müller-Gatermann, H. Ong, J. Song, and G. Wilson, *Nucl. Instrum. Methods Phys. Res., Sect. A* **1032**, 166612 (2022).
- [29] P. Carnelli, S. Almaraz-Calderon, K. Rehm, M. Albers, M. Alcorta, P. Bertone, B. Digiiovine, H. Esbensen,

- J. Fernández Niello, D. Henderson, C. Jiang, J. Lai, S. Marley, O. Nusair, T. Palchan-Hazan, R. Pardo, M. Paul, and C. Ugalde, *Nucl. Instrum. Methods Phys. Res., Sect. A* **799**, 197 (2015).
- [30] <https://web-docs.gsi.de/~weick/atima/>.
- [31] H. Jayatissa, M. L. Avila, K. E. Rehm, R. Talwar, P. Mohr, K. Auranen, J. Chen, D. A. Gorelov, C. R. Hoffman, C. L. Jiang, B. P. Kay, S. A. Kuvin, and D. Santiago-Gonzalez, *Phys. Rev. C* **105**, L042802 (2022).
- [32] M. Avila, K. Rehm, S. Almaraz-Calderon, A. Ayangeakaa, C. Dickerson, C. Hoffman, C. Jiang, B. Kay, J. Lai, O. Nusair, R. Pardo, D. Santiago-Gonzalez, R. Talwar, and C. Ugalde, *Nucl. Instrum. Methods Phys. Res., Sect. A* **859**, 63 (2017).
- [33] W.-J. Ong, M. L. Avila, P. Mohr, K. E. Rehm, D. Santiago-Gonzalez, J. Chen, C. R. Hoffman, Z. Meisel, F. Montes, and J. Pereira, *Phys. Rev. C* **105**, 055803 (2022).
- [34] R. Talwar, M. J. Bojazi, P. Mohr, K. Auranen, M. L. Avila, A. D. Ayangeakaa, J. Harker, C. R. Hoffman, C. L. Jiang, S. A. Kuvin, B. S. Meyer, K. E. Rehm, D. Santiago-Gonzalez, J. Sethi, C. Ugalde, and J. R. Winkelbauer, *Phys. Rev. C* **97**, 055801 (2018).
- [35] M. L. Avila, K. E. Rehm, S. Almaraz-Calderon, A. D. Ayangeakaa, C. Dickerson, C. R. Hoffman, C. L. Jiang, B. P. Kay, J. Lai, O. Nusair, R. C. Pardo, D. Santiago-Gonzalez, R. Talwar, and C. Ugalde, *Phys. Rev. C* **94**, 065804 (2016).
- [36] L. McFadden and G. Satchler, *Nucl. Phys.* **84**, 177 (1966).
- [37] P. Mohr, *Eur. Phys. J. A* **51**, 56 (2015).
- [38] See Supplemental Material at <http://link.aps.org/supplemental/10.1103/PhysRevLett.131.112701> for further information on the statistical analysis of the  $^{22}\text{Mg}(\alpha, p)^{25}\text{Al}$  reaction.
- [39] F. X. Haas and J. K. Bair, *Phys. Rev. C* **7**, 2432 (1973).
- [40] H. W. Drotleff, A. Denker, H. Knee, M. Soine, G. Wolf, J. W. Hammer, U. Greife, C. Rolfs, and H. P. Trautvetter, *Astrophys. J.* **414**, 735 (1993).
- [41] T. Rauscher (private communication).
- [42] G. Merz and Z. Meisel, *Mon. Not. R. Astron. Soc.* **500**, 2958 (2021).
- [43] P. Ubertini, A. Bazzano, M. Cocchi, L. Natalucci, J. Heise, J. M. Muller, and J. J. M. in 't Zand, *Astrophys. J. Lett.* **514**, L27 (1999).
- [44] R. Longland, C. Iliadis, and A. I. Karakas, *Phys. Rev. C* **85**, 065809 (2012).
- [45] J. W. Brümmner, P. Adsley, T. Rauscher, F. D. Smit, C. P. Brits, M. Köhne, N. A. Khumalo, K. C. W. Li, D. J. Marín-Lámbarri, N. J. Mukwevho, F. Nemulodi, R. Neveling, P. Papka, L. Pellegrini, V. Pesudo, B. M. Rebeiro, G. F. Steyn, and W. Yahia-Cherif, *Phys. Rev. C* **107**, 055802 (2023).
- [46] J. Browne *et al.* (JENSA Collaboration), *Phys. Rev. Lett.* **130**, 212701 (2023).
- [47] T. Rauscher, F.-K. Thielemann, and K.-L. Kratz, *Phys. Rev. C* **56**, 1613 (1997).
- [48] T. Rauscher and F.-K. Thielemann, *At. Data Nucl. Data Tables* **75**, 1 (2000).
- [49] M. Jaeger, R. Kunz, A. Mayer, J. W. Hammer, G. Staudt, K. L. Kratz, and B. Pfeiffer, *Phys. Rev. Lett.* **87**, 202501 (2001).
- [50] C. Angulo *et al.*, *Nucl. Phys.* **A656**, 3 (1999).
- [51] S. Ota, G. Christian, G. Lotay, W. Catford, E. Bennett, S. Dede, D. Doherty, S. Hallam, J. Hooker, C. Hunt, H. Jayatissa, A. Matta, M. Moukaddam, G. Rogachev, A. Saastamoinen, J. Tostevin, S. Upadhyayula, and R. Wilkinson, *Phys. Lett. B* **802**, 135256 (2020).
- [52] H. Jayatissa, G. Rogachev, V. Goldberg, E. Koshchiy, G. Christian, J. Hooker, S. Ota, B. Roeder, A. Saastamoinen, O. Trippella, S. Upadhyayula, and E. Uberseder, *Phys. Lett. B* **802**, 135267 (2020).
- [53] P. Adsley, U. Battino, A. Best, A. Caciolli, A. Guglielmetti, G. Imbriani, H. Jayatissa, M. La Cognata, L. Lamia, E. Masha, C. Massimi, S. Palmerini, A. Tattersall, and R. Hirschi, *Phys. Rev. C* **103**, 015805 (2021).
- [54] M. Wiescher, R. J. deBoer, and J. Görres, *Eur. Phys. J. A* **59**, 11 (2023).
- [55] P. Mohr, *Phys. Rev. C* **96**, 045808 (2017).
- [56] M. Basunia and A. Hurst, *Nucl. Data Sheets* **134**, 1 (2016).
- [57] C. Massimi *et al.* (n-TOF Collaboration), *Phys. Rev. C* **85**, 044615 (2012).
- [58] R. Firestone, *Nucl. Data Sheets* **110**, 1691 (2009).
- [59] P. Demetriou, C. Grama, and S. Goriely, *Nucl. Phys.* **A707**, 253 (2002).
- [60] V. Avrigeanu, M. Avrigeanu, and C. Măniulescu, *Phys. Rev. C* **90**, 044612 (2014).
- [61] P. Mohr, Z. Fülöp, G. Gyürky, G. G. Kiss, and T. Szücs, *Phys. Rev. Lett.* **124**, 252701 (2020).
- [62] P. Mohr, Z. Fülöp, G. Gyürky, G. Kiss, T. Szücs, A. Arcones, M. Jacobi, and A. Psaltis, *At. Data Nucl. Data Tables* **142**, 101453 (2021).
- [63] T. Rauscher, *Int. J. Mod. Phys. E* **20**, 1071 (2011).